JOURNAL OF APPLIED PHYSICS **118**, 155304 (2015)

Controlling the intrinsic bending of hetero-epitaxial silicon carbide micro-cantilevers

Atieh Ranjbar Kermany and Francesca Iacopi[a)]
Queensland Micro- and Nanotechnology Centre, Griffith University, Nathan, Queensland 4111, Australia

(Received 20 July 2015; accepted 3 October 2015; published online 20 October 2015)

We introduce a simple methodology to predict and tailor the intrinsic bending of a cantilever made of a single thin film of hetero-epitaxial silicon carbide grown on silicon. The combination of our novel method for the depth profiling of residual stress with a few nm resolution with finite element modelling allows for the prediction of the bending behaviour with great accuracy. We also demonstrate experimentally that a silicon carbide cantilever made of one distinct film type can be engineered to obtain the desired degree of either upward, flat, or downward bending, by selecting the appropriate thickness and cantilever geometry. A precise control of cantilever bending is crucial for microelectrical mechanical system applications such as micro-actuators, micro-switches, and resonant sensors. © *2015 AIP Publishing LLC*. [http://dx.doi.org/10.1063/1.4934188]

I. INTRODUCTION

Epitaxial cubic silicon carbide (3C-SiC) is a leading material for microelectrical mechanical systems (MEMS) due to its excellent mechanical properties when silicon (Si) has limitations.[1–4] Furthermore, it can be grown on Si substrate, which results in large area, easy micromachining, and low cost production.[5,6] However, the difference in Si and 3C-SiC lattice constants (∼20% mismatch) and thermal expansion coefficients (∼8% mismatch during the cool down) results in wafer bow and a high residual stress.[5,7]

The residual stress affects the mechanical behaviour of a thin film, and their consequence could be advantageous or detrimental depending on the application.[8] We have previously shown that high residual stress can improve the sensitivity parameter (frequency (f) × quality factor (Q)) of resonant microstrings,[6] which could be beneficial for applications such as resonant sensing. Whereas, stress-free microstructures are required for applications such as pressure sensors to prevent the stiffening effect.[9]

Residual stress can also result in the deformation of released microstructures. In the case of the single-clamped structures such as a cantilever, uniform (mean) residual stress within the film would be released because of the free end. However, if there is a variation of residual stress over the film thickness (gradient stress),[10] the structure will bend upon release.[7,11–14] This intrinsic bending could be applied favourably in MEMS thermal actuators such as normally closed micro-cages,[15] micro-wrappers,[16] micro-grippers,[17,18] and electrostatic actuators.[19,20] Similarly, the bending can greatly reduce the required voltage for MEMS switches.[21–23] However, flat structures are required in applications such as atomic force microscopy (AFM) and most resonant sensors.[24,25] As a result, it is important to understand, control, and engineer the intrinsic bending depending on the application.

Most literature reports have focused on the tuning of film deposition parameters to alter stress gradients[7,26] or metallization of the thin film[8,27,28] in order to manipulate the intrinsic bending of the released structures. Some also used multilayer structures in order to balance and control the intrinsic bending.[29,30] In this paper, we demonstrate the tailoring of the intrinsic bending of a single-layered cantilever made of hetero-epitaxial 3C-SiC on silicon by combining the knowledge of the film gradient stress (in nanometer (nm) resolution)[31] with finite element modelling (FEM). The stress gradient of a hetero-epitaxial 3C-SiC film is so complex that we can engineer 3C-SiC cantilevers to bend upward, downward, or to be nearly flat, even by just using one single film, by selecting the appropriate thickness and film type. We also study the influence of the cantilever geometry and the gravity on the degree of bending.

II. EXPERIMENT

3C-SiC films with thickness of 200–250 nm were grown on 150 mm silicon wafers with ⟨100⟩ and ⟨111⟩ surface orientations at 1000 °C in a hot-wall horizontal low-pressure chemical vapour deposition chamber, using silane (SiH_4) and propene (C_3H_6) as precursor gases.[32] The thickness was measured using Veeco Wyko NT1100 optical profilometer, which has a resolution of 1 Å, assuming a constant refractive index of 2.65 for 3C-SiC films.[33] The stresses were calculated from the wafer warpage measured with a Tencor Flexus 2320 system. The gradient stresses throughout the SiC films thickness were calculated over monitoring the wafer curvature by etching back the films through sequential steps of ∼10–20 nm thickness, as detailed in our previous work.[31] The Young's modulus (E) was calculated using Hysitron Triboindenter nanoindentation on 1 μm thick films. It should be noted that E might be affected by the defect density and so it is not necessarily uniform throughout the thickness.[34–36] With the assumption that the Young's modulus is constant throughout the thickness, we calculated values of 400 GPa and 330 GPa for SiC(111) and SiC(100),

[a)]Electronic mail: f.iacopi@griffith.edu.au

respectively.[32] As the result of this assumption, the residual stress values may be somewhat overestimated.

The different SiC film thicknesses studied in this work were obtained by etching back the 250 thick films after their deposition. For this purpose, we used an inductively coupled plasma (ICP) STS anisotropic etcher with a flow of 50 sccm hydrogen chloride (HCl) at 4 mTorr and room temperature to perform the etching. SiC thickness uniformity remained around 2% with 3–5 nm variation across the 150 mm wafer.[37]

We fabricated the cantilevers using Si surface micromachining and through the four stages of photolithography, SiC etching (STS etcher), Si etching (using xenon difluoride (XeF_2) isotropic dry chemical etcher), and photoresist removal (using TEGAL 915 oxygen plasma with 1200 mTorr pressure, 100 °C temperature, and 550 W RF power). We used two photolithography steps in order to release the structures perfectly clamped. We used the first lithography step to develop the cantilever patterns on SiC film. Subsequently, we used the second lithography step after the SiC etching and prior to the Si etching in order to protect the cantilever anchors from overetching due to the isotropic behaviour of the XeF_2 etching process. The details on perfectly clamped fabrication method can be found in our previous work.[6]

We analysed the intrinsic bending by comparing the FEM analysis to the scanning electron microscopy (SEM) micrographs of experimentally fabricated cantilevers. The SEM was performed with a JEOL JSM-6510 LV. We performed the FEM analysis using the IntelliSuite software (version 8.7). The cantilevers were designed and their intrinsic bending was analysed using the 3DBuilder and the Thermo-Electro-Mechanical (TEM) modules of the software. The Young's modulus, Poisson's ratio (ν), density (ρ), and residual were inserted in the TEM module for the analysis. The Poisson's ratio values of 0.235 for SiC(111) and 0.267 for SiC(100) and density of 3.21 g cm^{-2} were taken from literature.[3,38] The SiC residual stress was input by subdividing the modelled 3C-SiC films into multiple nm thick layers. The stress of each thin layer was assigned according to the layer-by-layer stress profiles of our recent work[31] (Fig. 1).

III. RESULTS AND DISCUSSION

A. Stress relaxation mechanism upon growth

The epitaxial growth of 3C-SiC on silicon typically leads to high residual tensile film stresses, due to a combination of lattice and thermal mismatches. The stress arising from the thermal mismatch is not expected to contribute to stress gradients, as it is only related to the cooling phase after the film growth.[3,10,12] The overall film residual mean stress, as well as the stress gradient behaviour and resulting defect densities, depend strongly on the chosen deposition conditions, as they are directly linked to the stress relaxation rates upon film growth.[10]

Even though the strain produced from the lattice and thermal mismatches can be considered independent of the Si orientation, we have reported that the relaxation over thickness (gradient stress) is faster in SiC(100) as compared to SiC(111) when using the same film growth process.[31] This is due to the fact that the density of the stacking faults (SFs), which are one of the dominant stress relaxation mechanisms in 3C-SiC films,[12,37] are more efficient in SiC(100) films because of their more favourable geometrical projection onto the ⟨100⟩ Si growth plane.[31,32]

Figures 1(a) and 1(b) show a typical stress gradient depth profile for the SiC(100) and SiC(111) films, respectively, measured with high resolution as discussed in our previous work.[31] Both SiC films show a highly compressed nanolayer at the interface with the substrate, which we had attributed to the out-diffusion of silicon in the carbonization layer.[31] This could also be linked to the super cell mismatch between SiC and Si pointed out by Zielinski *et al.*[10] As the growth proceeds, both films quickly build up a tensile stress due to the thermal mismatch contribution. This results in a sharp positive (tensile) *gradient*. This tensile gradient continues until both films reach about 500 MPa of tensile stress, around 20–30 nm thickness. Interestingly, while the SiC(111) film retains that value of tensile stress throughout the remaining thickness, as thickness increases beyond ~35 nm, the SiC(100) film stress starts to relax resulting in a negative (compressive) gradient. The stress of the topmost layers of the SiC(100) film evolves towards full relaxation (stress value approaching 100 MPa). Consequently, the stress gradient behaviour versus thickness can be divided to two regions, a highly tensile followed by a slightly compressive region for the SiC(100) film and a highly tensile region followed by an almost flat plateau for the SiC(111) film, as shown in Figs. 1(a) and 1(b), respectively. Note that this analysis was limited to relatively thin SiC films; larger thicknesses are required to further examine the relaxation rate in SiC(111) film.

In a single-layer cantilever, the stress gradients within the single layer are responsible for the intrinsic bending. Thus, the direction of the cantilever bending is influenced by the gradient stress state.

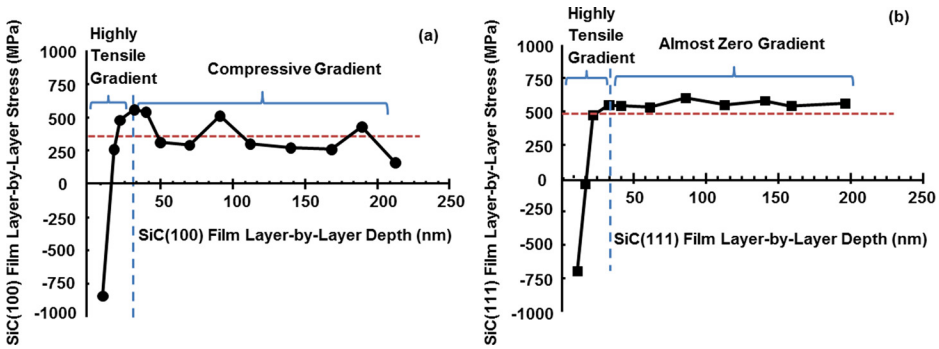

FIG. 1. Layer-by-layer stress profile; stress gradient regions for on-axis (a) SiC(100) and (b) SiC(111).[31] SiC(100) have a tensile gradient and a compressive gradient region above ~35 nm thickness, resulting from film relaxation, while the SiC(111) shares the same initial tensile gradient but shows a nearly flat behaviour (nearly zero gradient) thereafter. The red dotted line is added only to guide the eye.

For the SiC(100) films, we observe upward bending for thicknesses up to ~77 nm because the dominant gradient stress is tensile. Figures 2(a) and 2(b) show FEM and SEM results, respectively, obtained for a SiC(100) cantilever with the thickness of 66 nm. The FEM image (Fig. 2(a)) shows an upward deflection of ~60 μm. The value is in good agreement with the fabrication result (Fig. 2(b)), validating the model based on the measured gradient data.

At 77 nm thickness, the FEM analysis predicts nearly zero bending for the SiC(100) cantilever. At this point, the compressive and tensile stress gradients are almost equal and so the cantilever is flat. Indeed, for thicknesses slightly above 77 nm, we start observing experimentally downward bending for the SiC(100) cantilever. Figures 2(c) and 2(d) show the FEM analysis and a SEM image of a SiC(100) cantilever with the thickness of 80 nm. The SEM image (Fig. 2(d)) shows slightly downwards bending, which is in good agreement with the FEM result (bending of ~3 μm). The downward bending happens due to the fact that the dominant gradient starts to be the compressive one.

The degree of downward bending increases as thickness increases to 250 nm because the compressive gradient stress increases. Figures 2(e) and 2(f) are FEM and SEM images of a SiC(100) cantilever with the thickness of 250 nm. A negative bending of ~60 μm can be observed through the FEM result (Fig. 2(e)), which is again in good agreement with the fabrication result (Fig. 2(f)).

As for the SiC(111) cantilever, the bending behaviour is similar to the SiC(100) cantilever for the highly tensile region. In addition, the bending remains upward for any thickness up to the maximum investigated here because the stress gradient remains tensile throughout. Figures 3(a) and 3(b) show the deflection comparison between SiC(100) and SiC(111) cantilevers with 250 nm thickness.

Overall, we observe upward, flat, and downward intrinsic bending in SiC(100) cantilever but only upward bending for SiC(111) cantilever for thicknesses up to 250 nm, due to the difference in their stress relaxation rate. Consequently, engineering the thin film cantilever bending to three forms of upward, flat, and downward is only possible through the ⟨100⟩ orientation.

Note that this finding is potentially in agreement with the work by Zielinski *et al.*[39–41] They investigated cantilever bending for SiC with thicknesses from 100 nm to above 1 μm and shown constant upward bending in SiC(111) as we report, but only downward bending in SiC(100). As we show here, the upward bending of SiC(100) is restricted to a narrow region, i.e., films thinner than 80 nm. In the light of our findings, it is likely that upward bending would have been observed only for films thinner than those they have analysed.

B. Cantilever geometry

The degree of bending can be further influenced by the cantilever geometry and the 3C-SiC elastic properties. The

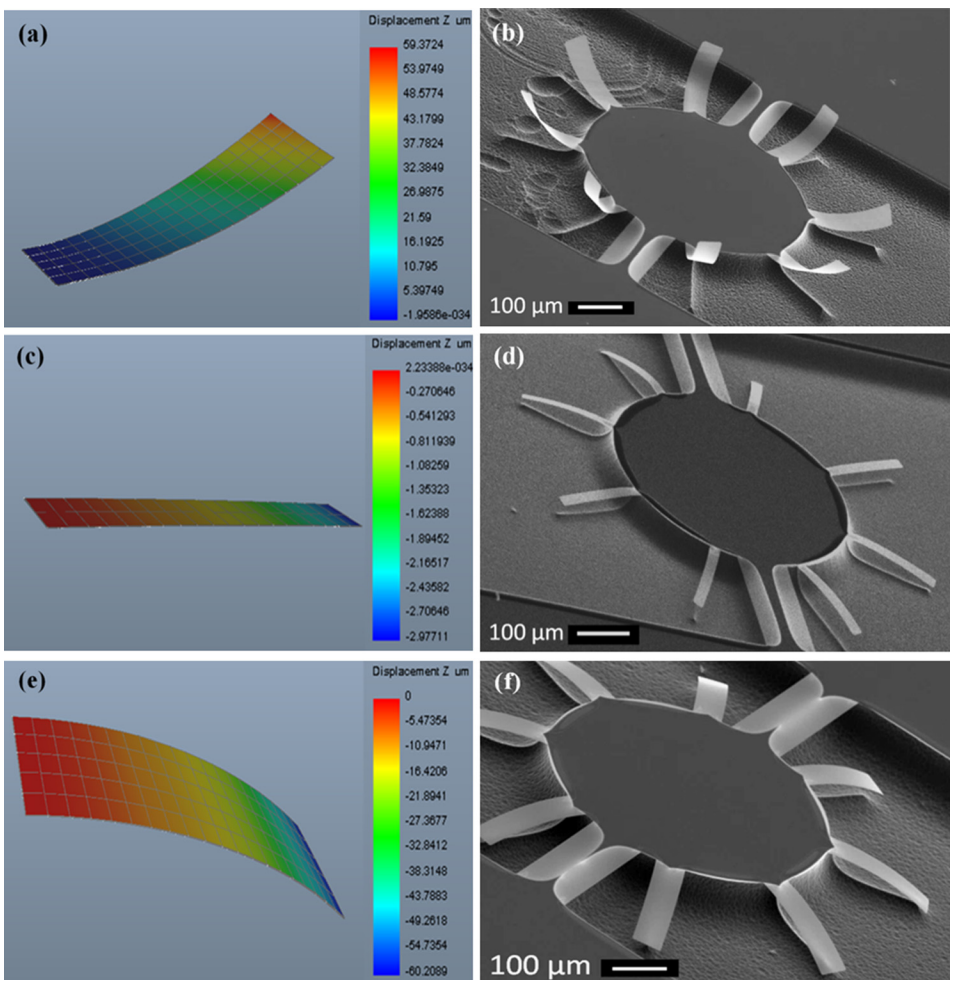

FIG. 2. SiC(100) cantilevers with 200 μm length bending behaviour: upward bending due to the tensile gradient region (a) FEM and (b) SEM results (50 μm width, and 66 nm thickness); nearly flat region (c) FEM and (d) SEM images (20 μm width, and 80 nm thickness); and downward bending due to the compressive gradient region (e) FEM and (f) SEM results (50 μm width, and 250 nm thickness). The SEM images are taken with 60° tilting.

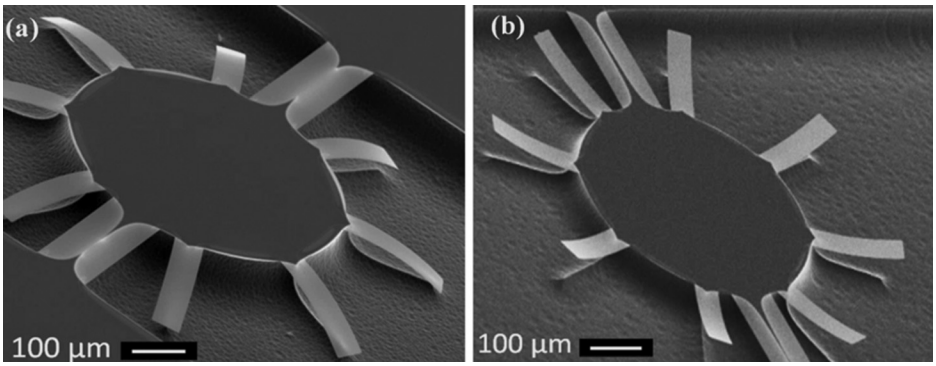

FIG. 3. Intrinsic bending comparison of cantilevers made of (a) SiC(100) and (b) SiC(111), with length of 200 μm, width of 50 μm, and thickness of 250 nm. The SEM images are taken with 60° tilting.

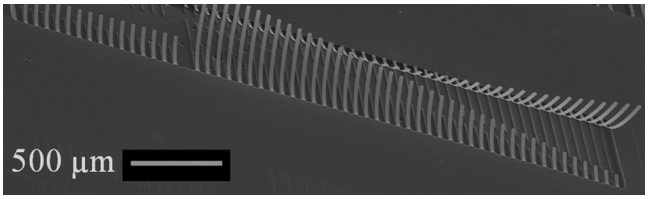

FIG. 4. SEM image of SiC(111) cantilevers with varying length (100 μm to 1000 μm), width of 20 μm, and thickness of 250 nm. The SEM image is taken with 60° tilting.

maximum vertical deflection (δ) of the cantilever can be described by[42]

$$\delta = \frac{M(1-\nu)l^2}{2EI}, \tag{1}$$

where M is the bending moment and l is the cantilever length. I is the inertia momentum (rectangular cross section: $I = (wt^3)/12$, where w and t are the cantilever width and thickness, respectively).[7,25] When assuming a linear stress gradient, $M = \sigma_1 I$ can be used, and therefore, the effect of the cantilever width can be neglected.[42]

We can see from Eq. (1) that the vertical deflection is directly affected by the cantilever length (l).[14,43–45] This is also evident in Fig. 4. Thus, the cantilever geometry affects the degree of upward or downward bending but it does not initiate the deflection. As mentioned, the origin of the cantilever intrinsic bending is the stress gradient.

C. Gravity

The degree of bending can also be influenced by the gravity. We calculated the vertical deflection of the 3C-SiC cantilever (with different geometries) due to gravity through the following equation:[7]

$$\xi = \frac{wt\rho l^4}{8EI}, \tag{2}$$

where ξ is the cantilever deflection due to the gravity. We find the cantilevers maximum deflection due to the gravity in small picometer (pm) ranges. Consequently, the gravity effect on the 3C-SiC cantilever vertical deflection can be ignored.

IV. CONCLUSION

This work brings important insights on the cantilever intrinsic bending behaviour. We demonstrated a simple method to predict, control, and engineer the intrinsic bending of a single-layered 3C-SiC cantilever by selecting the appropriate film type, thickness, and cantilever length. We predicted the cantilever intrinsic bending behaviour with great accuracy through the FEM simulation combined with the measured film stress gradient (in nm resolution). In addition, we confirmed experimentally that upward, flat, or downward bending with desired degrees could be obtained for SiC(100) cantilevers by selecting the thickness in the appropriate regions. We also confirmed that the degree of bending can be further adjusted by varying the cantilever length. This way we can tailor the bending direction and degree to the targeted application. Deflected cantilevers with desired bending degrees can be used for MEMS applications such as micro-actuators and micro-switches, whereas flat cantilever is mainly preferred for resonant sensors.

ACKNOWLEDGMENTS

Fabrication was performed using the equipment of the Australian National Fabrication Facilities (ANFF), Queensland node. We thank Marcin Zielinski from NovaSiC for helpful discussion and Neeraj Mishra from Griffith University for experimental support. The authors acknowledge the support from AFOSR through the AOARD 15IOA053 Grant. Associate Professor F. Iacopi is the recipient of an Australian Research Council Future Fellowship (FT120100445).

[1]N. G. Wright and A. B. Horsfall, J. Phys. D: Appl. Phys. **40**(20), 6345 (2007).
[2]C. A. Zorman and R. J. Parro, Phys. Status Solidi B **245**(7), 1404 (2008).
[3]V. Cimalla, J. Pezoldt, and O. Ambacher, J. Phys. D: Appl. Phys. **40**(20), 6386 (2007).
[4]B. V. Cunning, M. Ahmed, N. Mishra, A. R. Kermany, B. Wood, and F. Iacopi, Nanotechnology **25**(32), 325301 (2014).
[5]A. Severino, C. Locke, R. Anzalone, M. Camarda, N. Piluso, A. La Magna, S. Saddow, G. Abbondanza, G. D'Arrigo, and F. La Via, ECS Trans. **35**(6), 99 (2011).
[6]A. R. Kermany, G. Brawley, N. Mishra, E. Sheridan, W. P. Bowen, and F. Iacopi, Appl. Phys. Lett. **104**(8), 081901 (2014).
[7]R. Anzalone, M. Camarda, C. Locke, D. Alquier, A. Severino, M. Italia, D. Rodilosso, C. Tringali, A. La Magna, and G. Foti, J. Electrochem. Soc. **157**(4), H438 (2010).
[8]J. Pezoldt, R. Nader, F. Niebelschütz, V. Cimalla, T. Stauden, C. Zgheib, and P. Masri, Phys. Status Solidi A **205**(4), 867 (2008).
[9]F. Niebelschütz, K. Brueckner, V. Cimalla, M. A. Hein, and J. Pezoldt, Mater. Sci. Forum **615–617**, 621 (2009).
[10]M. Zielinski, A. Leycuras, S. Ndiaye, and T. Chassagne, Appl. Phys. Lett. **89**, 131906 (2006).

[11]R. Anzalone, G. D'arrigo, M. Camarda, C. Locke, S. E. Saddow, and F. La Via, J. Microelectromech. Syst. **20**(3), 745 (2011).
[12]M. Bosi, B. E. Watts, G. Attolini, C. Ferrari, C. Frigeri, G. Salviati, A. Poggi, F. Mancarella, A. Roncaglia, and O. Martínez, Cryst. Growth Des. **9**(11), 4852 (2009).
[13]B. Van Drieënhuizen, J. Goosen, P. French, and R. Wolffenbuttel, Sens. Actuators, A **37–38**, 756 (1993).
[14]M. Lishchynska, N. Cordero, O. Slattery, and C. O'Mahony, J. Micromech. Microeng. **15**(7), S10 (2005).
[15]J. K. Luo, R. Huang, J. H. He, Y. Q. Fu, A. J. Flewitt, S. M. Spearing, N. A. Fleck, and W. I. Milne, Sens. Actuators, A **132**(1), 346 (2006).
[16]J. Gill, D. T. Chang, L. A. Momoda, and G. P. Carman, Sens. Actuators, A **93**(2), 148 (2001).
[17]Y. Bellouard, Mater. Sci. Eng., A **481–482**, 582 (2008).
[18]Y. Fu, H. Du, W. Huang, S. Zhang, and M. Hu, Sens. Actuators, A **112**(2), 395 (2004).
[19]J. Musolf and P. Kohl, U.S. patent 6,625,004 (2003).
[20]G. D. Gray, M. J. Morgan, and P. A. Kohl, "MEMS components and applications for industry, automobiles, aerospace, and communication II," Proc. SPIE **4981**, 202 (2003).
[21]P. Schmid, F. J. Hernandez-Guillen, and E. Kohn, Diamond Relat. Mater. **12**(3), 418 (2003).
[22]R. T. Chen, H. Nguyen, and M. C. Wu, IEEE Photon. Technol. Lett. **11**(11), 1396 (1999).
[23]D. Peroulis, K. Sarabandi, and L. Katehi, in *2002 IEEE MTT-S International Microwave Symposium Digest* (IEEE, Seattle, WA, USA, 2002), Vol. 1, pp. 223.
[24]N. V. Lavrik, M. J. Sepaniak, and P. G. Datskos, Rev. Sci. Instrum. **75**(7), 2229 (2004).
[25]A. Boisen, S. Dohn, S. S. Keller, S. Schmid, and M. Tenje, Rep. Prog. Phys. **74**(3), 036101 (2011).
[26]F. J. Hernandez-Guillen, K. Janischowsky, J. Kusterer, W. Ebert, and E. Kohn, Diamond Relat. Mater. **14**(3), 411 (2005).
[27]C. Zgheib, P. M. Masri, P. Weih, O. Ambacher, and J. Pezoldt, Mater. Sci. Forum **457–460**, 301 (2004).
[28]J. Pezoldt, T. Stauden, F. Niebelschütz, M. A. Alsioufy, R. Nader, and P. M. Masri, Mater. Sci. Forum **645–648**, 159 (2010).
[29]M. A. Matin, K. Ozaki, D. Akai, K. Sawada, and M. Ishida, Comput. Mater. Sci. **85**, 253 (2014).
[30]L. Wen, H. Zeng, Z. Yuan, J. Chu, and H. Wang, in , *2011 IEEE International Conference on Nano/Micro Engineered and Molecular Systems (NEMS)* (IEEE, 2011), pp. 634.
[31]F. Iacopi, R. E. Brock, A. Iacopi, L. Hold, and R. H. Dauskardt, Acta Mater. **61**(17), 6533 (2013).
[32]F. Iacopi, G. Walker, L. Wang, L. Malesys, S. Ma, B. V. Cunning, and A. Iacopi, Appl. Phys. Lett. **102**(1), 011908 (2013).
[33]S. Singh, J. R. Potopowicz, L. G. Van Uitert, and S. H. Wemple, Appl. Phys. Lett. **19**(3), 53 (1971).
[34]R. Anzalone, M. Camarda, A. Canino, N. Piluso, F. La Via, and G. D'Arrigo, Electrochem. Solid-State Lett. **14**(4), H161 (2011).
[35]B. Hähnlein, M. Stubenrauch, S. Michael, and J. Pezoldt, Mater. Sci. Forum **778–780**, 444 (2014).
[36]B. Hähnlein, M. Stubenrauch, and J. Pezoldt, Mater. Sci. Forum **821–823**, 281 (2015).
[37]N. Mishra, L. Hold, A. Iacopi, B. Gupta, N. Motta, and F. Iacopi, J. Appl. Phys. **115**(20), 203501 (2014).
[38]H. Yao, L. Ouyang, and W. Y. Ching, J. Am. Ceram. Soc. **90**(10), 3194 (2007).
[39]M. Zielinski, J. F. Michaud, S Jiao, T. Chassagne, A. E. Bazin, A. Michon, M. Portail, and D. Alquier, Mater. Sci. Forum **679–680**, 79 (2011).
[40]S. Jiao, M. Zielinski, J. F. Michaud, T. Chassagne, M. Portail, and D. Alquier, Mater. Sci. Forum **711**, 84 (2012).
[41]M. Zielinski, J. F. Michaud, S. Jiao, T. Chassagne, A. E. Bazin, A. Michon, M. Portail, and D. Alquier, J. Appl. Phys. **111**, 053507 (2012).
[42]A. Ballestra, A. Somà, and R. Pavanello, Sensors **8**(2), 767 (2008).
[43]M. Camarda, R. Anzalone, A. Severino, N. Piluso, A. La Magna, and F. La Via, Mater. Sci. Forum **679–680**, 213 (2011).
[44]M. Camarda, R. Anzalone, A. Severino, N. Piluso, A. Canino, F. La Via, and A. La Magna, J. Mater. Res. **28**(01), 104 (2013).
[45]W. Fang, C. Lee, and H. Hu, J. Micromech. Microeng. **9**(3), 236 (1999).